ANALYSIS OF THE TEMPERATURE DISTRIBUTION IN FRICTION STIR WELDING OF AA 2024-T3 AND AA 6061-T6 USING FINITE ELEMENT METHOD

Sabah KHAMMASS HUSSEIN[1]

Different Aluminum alloys (AA 2024-T3 and AA 6061-T6) are welded by means of friction stir welding (FSW) with a wide range of linear and rotating speed. A finite element model is build using (COMSOL) program with the aid of heat transfer equations between the tool and specimen. The temperature distribution is recorded experimentally and compared with the finite element model. A good agreement is observed between the two methods. The higher temperature field found along the weld line behaves as a flame. Different material properties gave non-symmetrical temperature distribution about the weld line in the upper surface. The increase of the linear and rotating speed results in decreasing and increasing the temperature respectively. At low welding speed, the higher rotating speed has no effect on temperature. Increasing the rotating speed results in transmission of the higher field of temperature distribution from the region of low melting point material to other. The higher temperature distribution field is found in the contact area between shoulder and specimen. The lower and symmetrical temperature distribution is located in the lower surface of specimen as comparing with upper surface.

Keywords: FSW, FEM, Temperature distribution, dissimilar materials.

1. Introduction:

During the welding process, the heat flow change the microstructure and mechanical properties of weld metal and heat affected zone. Residual stresses and distortion are induced. The temperature distribution starts with high values at weld metal and decreases gradually [1]. A fully coupled thermo-mechanical FE is developed in FSW taking into account the plastic deformation and recrystallization in nugget zone. Good agreement is found between the measured residual stresses and calculated from the finite element model [2].

Different tool geometry is used to weld dissimilar metal by FSW. The tool geometries are modeled using FEM by ANSYS program. The weld quality is affected by the tool geometry.

The least heat flux is generated by concave fluted tool geometry. A non-uniform heat flux is generated in the threaded tool geometry. A greater heat flux is found in taper as comparing with the threaded tool geometry [3]. A FEM model of FSW is build depending on Re- Normalization Group (RNG) k-□□model. They

[1] Ass Prof. Engineering Technical College – Baghdad, Middle Technical University, Iraq- Baghdad. E-mail: sabah.kh1974@yahoo.com.

conclude that the direction of rotating speed and flow material near the tool is the same. The shoulder region gave a higher metal flow velocity. The dimension of tool shoulder and pin has no effect on the direction of metal flow [4].

Using the Rosenthal model, a FE model is developed to study the heat flow in FSW. The heat transfer, continuum mechanics and material flow are considered. The measured temperature distribution gave a good agreement as comparing with the FE model [5]. A theoretical model for the temperature distribution in the weldment is proposed depending on the Gaussian heat sources model. One can conclude that the thermal cycles obtained from this model are more reliable than those obtained from the concentrated heat source model [6].

2. Experimental work

2.1 Properties and dimensions of specimens and tool

Two dissimilar Aluminum materials are welded by FSW; the first one is 2024-T3 and the other is 6061-T6. The chemical composition for each material is listed in Table 1:

Table 1

Chemical composition of AA2024-T3 and AA6061-T6

Element	wt%	Cr	Cu	Ti	Fe	Si	Mn	Mg	Zn	AL
AA2024-T3	Measured	0.005	4.0	0.021	0.2	0.36	0.6	1.4	0.071	Rem.
	Standard [7]	0.10	4.9	0.15	0.50	0.50	0.9	1.8	0.25	Rem.
AA6061-T6	Measured	0.206	0.329	0.019	0.46	0.643	0.099	0.888	0.114	Rem.
	Standard [7]	0.04 to 0.3	0.15 to 0.4	Max 0.15	Max 0.7	0.4 to 0.8	Max 0.15	0.8 to 1.2	Max 0.25	95.8 to 98.6

The tensile test properties for each material are obtained from a standard tensile test specimen, ASTM B557-02a [8]. Table 2 presents these properties:

Table 2

Mechanical properties of AA2024-T3 and AA6061-T6

Material		Yield stress (MPa)	Tensile stress (MPa)
2024-T3	Measured	300	445
	Standard [7]	289 Min.	434 Min.
6061-T6	Measured	288	320
	Standard [7]	276	310

Two specimens with the dimensions 150 mm length, 75 mm width and 3 mm thickness, are welded by means of tool (O1 tool steel type), ASTM A681 [9], Fig. 1. The probe height and diameter are 2.8 and 3 mm, respectively.

2.2 Welding parameters

The welding process parameters have an effect on the quality of welding. The linear and rotating speed of machine must be controlled in order to reduce flash and void.

These parameters have an effect on the microstructure and temperature distribution of weldment. In this work, a wide range of linear and rotation welding speed are used, see Table 3.

Table 3

Linear and rotating welding speeds

Linear speed (mm)	2	5	10	15	20	25	30	35
Rotating speed (RPM)	250	500	750	1000	1250	1500	1750	2000

Each case of linear speed test is used with all cases of rotating speed, such that the total tested cases are 64. Fig. 2 shows the measurement of the temperature by means of a thermocouple device during FSW.

Fig. 1. Photograph of tool

3. Finite element modeling of friction stir welding

3.1 Heat transfer in friction stir welding

The start of the finite element formulation is based on the moving heat source through the welded plate. The temperature distribution through welding process is calculated according to *Navier*- equation [10].

A combined of convection and conduction heat transfer occurred during the welding process. The steady state condition with respect to moving heat source is presented by Eq (1), [11]:

$$\nabla.(-k\,\nabla T) = Q - \rho\, C_p\, u\,.\nabla T \qquad (1)$$

where: k is the thermal conductivity (W/m·K), T is the temperature [K], ρ-is the density [kg/ m^3], C_p is the specific heat capacity [J/kg·K] and u is the linear velocity of heat source [m/s].

A sample of the welded specimen is shown in Fig. 3.

The pin in tool is considered as the heat source during the friction stir welding. It is assumed that the generated conductive heat transfer model in the common interface between the pin and the welded plate is [12]:

$$q_{pin}(T) = \frac{\mu}{\sqrt{3(1+\mu^2)}}\, r_p\, \omega \bar{Y}(T) \tag{2}$$

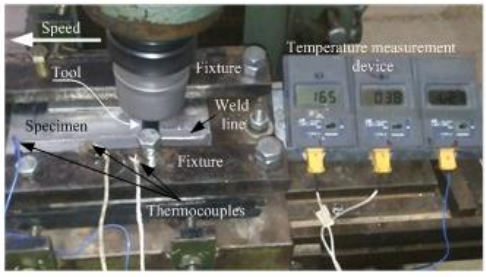

Fig. 2. Temperature measurements during friction stir welding process

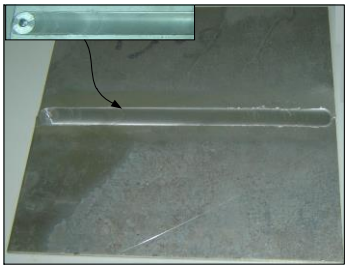

Fig. 3. Sample of welded specimen by friction stir welding

where q_{pin} is the generated heat between pin and workpiece [W/m^2], μ - is the coefficient of friction between pin and workpiece, r_p is the radius of pin [m], ω is the angular velocity of pin [Rad/s] and $\bar{Y}(T)$ is the average shear stress of the welded specimens [MPa]. The generated heat at the interface between the lower surface of the rotated shoulder and the welded specimens yields due to friction between them. The following formula is presented [12]:

$$q_{shoulder}(r,T) = \begin{cases} \left(\mu\frac{F_n}{A_s}\right)\omega r & T < T_{melt} \\ 0 & T \geq T_{melt} \end{cases} \tag{3}$$

where $q_{shoulder}$ is the generated heat between shoulder and work piece [w/m^2], r is the distance from the center of tool [m], F_n is the normal force of tool [N], A_s is the surface area of shoulder [m^2] = $\pi\,(r^2_{pin} - r^2_{shoulder})$, and T_{melt} is welded specimens melting temperature [K].

A combination of convection and radiation are lost from the surfaces of welded plate. The surrounding of upper surface differs from that of the lower surface. Therefore, the heat transfer for each surface will be [13]:

$$q_{up} = h_{up}\,(T_O - T) + \epsilon\sigma\,(T^4_{amb} - T^4) \tag{4}$$

$$q_{down} = h_{down}\,(T_O - T) + \epsilon\sigma\,(T^4_{amb} - T^4) \tag{5}$$

where q_{up}&q_{down} are the heat loss from upper and lower surface of workpiece respectively [W/m^2], h_{up}&h_{down} is the convection coefficient of upper and lower surface of workpiece [w/m^2·K], T_O & T_{amb} are the initial and ambient temperature [K], ε is the surface emissivity, and σ is the Stefan-Boltzmann constant [W/m^2·K^4].

3.2 The finite element model

The distribution of temperature through the welded plate is calculated using the finite element method with the aid of the COMSOL Multiphysics 4.3 software, as follows:

Building of the model consists in creation of geometrical entities which include the volumes of the actual problem geometry. The model is build such that the center of tool is located at the original point of the basic axis, Fig. 4a. A mesh of the model is created with quadratic elements for each plate and triangle elements for pin and shoulder; Fig. 4b.

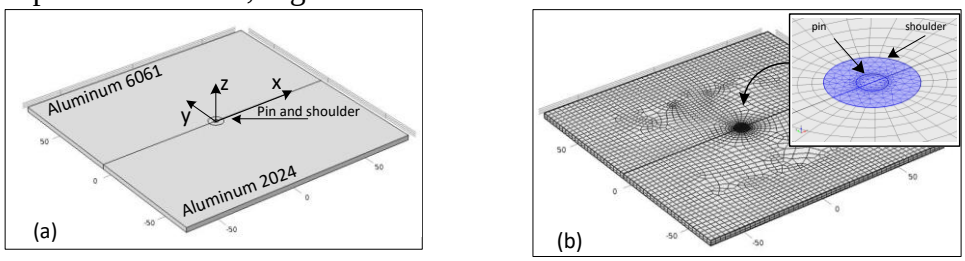

Fig. 4. Problem model (a) geometry (b) mesh

This heat transfer generation model represents the definition of the generated heat transfer rate (q) in each boundary of pin and shoulder. The generated heat transfer rate in pin (q_{pin}), Eq (2)., is applied in the boundaries (1 & 2), Fig. 5. The heat equation contains the average shear stress of the welded specimen which has a different function for each material. In this work, a different material of the welded specimen is used (*Al 6061* and *Al 2024*). Each material has a specific function of shear stress and therefore, the heat rate will differ from one to the other according to the bounded region between the pin surface area and each material. The generated heat in the first half of pin surface area (boundary 1), which is in contact with the material *Al 6061*, will be Eq(2). such that the average shear stress will be of material *Al 6061*. The generated heat in the second half of pin surface area (boundary 2), which is in contact with the material *Al 2024*, will be Eq(2). such that the average shear stress will be of material *Al 2024*.

The generated heat transfer rate in shoulder ($q_{shoulder}$), Eq (3), depends on the melting point of material. This equation is applied in the first lower half of shoulder area (boundary 3) which is in contact with the material *Al 6061*, such that the melting point will be of material *Al 6061*. Also, this equation is applied in the second lower half of shoulder area (boundary 4) which is in contact with the material *Al 2024*, such that the melting point will be of material *Al 2024*, Fig. 6. The heat lost from the model consists of convection and radiation from the upper and lower surface are found using Eqs (4). and (5). The upper heat lost in Eq (4). is applied on the shaded area of the upper surface, Fig. 7. This region represents the upper surface area of the two welded specimens minus the area of pin and shoulder

which have no heat lost. On the other hand, the lower heat lost in Eq (5) is applied on the shaded area of the lower surface which includes the lower surface area of the two welded specimens minus the area of pin only. The values of upside and downside convection coefficient are 12.25 and 6.25 W/m^2· K respectively [14]. The ambient temperature is taken as T_O = 300 K.

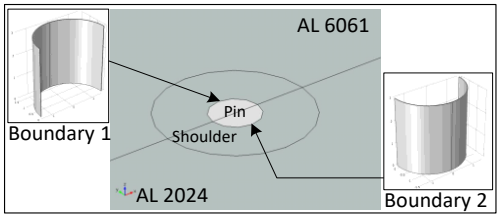

Fig. 5. Pin heat boundaries

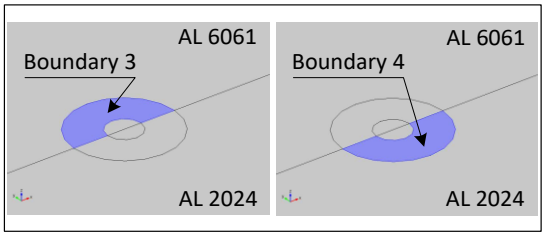

Fig. 6. Shoulder heat boundaries

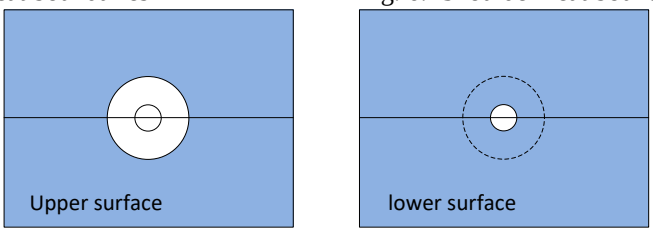

Fig. 7. Heat flux boundaries for the upper and lower surface

3.3 Thermal properties

In order to solve this model, the following material properties shown in Table 4 are required, [8].

Table 4

Thermal material properties of welded specimens and tool

Property	AA6061-T6	AA2024-T3	tool
Thermal conductivity [W/m·K]	167	120	42
Heat capacity [J/Kg·K]	896	875	500
Melting point [K]	933	775	
Surface emissivity [14]	0.3	0.3	

4. Results and discussion

This study analyzes the temperature distribution when the tool reaches the center point of welded specimen, Fig. 4. In order to validate the obtained values of the temperature distribution along the weld line for the proposed model using experimental measurements, a simple (3D) numerical result is illustrated in Fig. 8. The conditions of this case is v= 25 mm/s, N= 250 rpm). The higher temperature field is found at the region of tool and decreased gradually in the direction of linear welding speed. The shape of temperature distribution behaves like flame starts from the center of rotating tool toward the region of welded specimen in the direction of

linear speed. The maximum temperature value is 500 K near the weld zone and reach the ambient temperature 300 K near the weldment specimen edge. As it has been observed, a good agreement is found between the results of the FE model and the experimental data. The higher rate in temperatures change is found along the weld line (x-axis) as compared with the transverse line (y-axis). This phenomenon can be explained by the fact that the higher friction occurred along the axis of linear speed. Due to higher generated heat near the weld line, a sharp increase in temperature is found in this region.

The values of temperature distribution along the y-axis for all cases mentioned in Table 3 are illustrated in Figs. 9 to16. The negative and positive values of the y-axis represent the region of materials (AL2024 and AL6061) respectively.

Generally, the temperature has a maximum value at the weld metal and decrease gradually through the heat affected zone until the weldment edge away from the y-axis. The different properties of the welded materials (AL6061, AL2024) gave a non-symmetrical temperature distribution about the x-axis. Increasing the linear velocity gives a decrease of the temperature values. This phenomenon is clear at low rotating speed. Hence, for N= 250 rpm, higher temperature values along the y-axis are found at *v*= 2 mm/s, Fig. 9, which decrease until it reaches the minimum values at maximum speed, Fig. 16. The decrease of the linear velocity means that more time is required to complete the welding process and therefore, the friction time will increase. This increases the heat generated and temperature values.

At lower linear speed, the higher rotating speeds have no effect on the increasing of temperature, Figs. 9 and 10. Hence, at *v* = 2 and 5 mm/s, the temperatures distribution is approximately the same for rotational speed range from 750 to 2000 rpm).

It is observed that the higher rotating speeds ranging from 1250 to 2000 rpm, gave the same temperatures distribution at the higher values of linear speed values ranging from 2 to 35 mm/s.

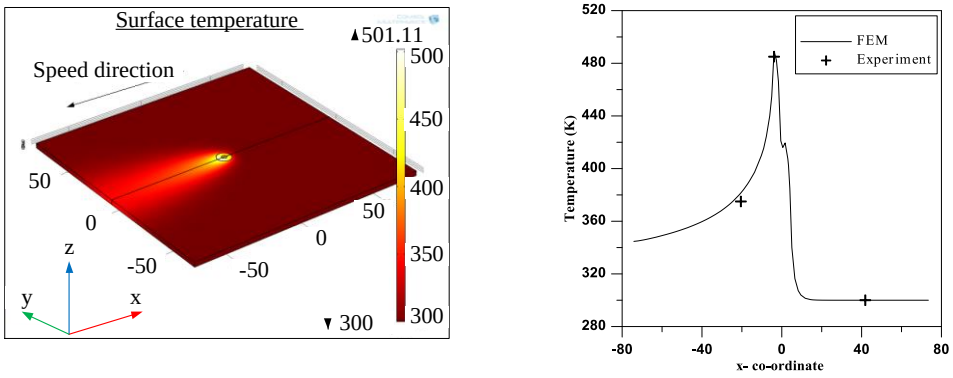

Fig. 8. Temperature distribution along the weld line, v =25 mm/sec, N=250 RPM

4.1 Temperature distribution in the circle region of pin and shoulder

This region includes the weld line and the heat affected zone (HAZ). At low rotating speed, N=250 rpm, and for all range of the linear speed, the higher temperature distribution observed at the region of lower melting point material *Al2024* as comparing with that of higher melting point material *Al6061*, Figs. 9 to 16.

At high rotating speed from 1250 to 2000 rpm, and for all range of linear speed, the higher temperature distribution observed at the region of higher melting point material *Al6061* as comparing with that of higher melting point material *Al2024*.

For the other intermediate rotating speed from 500 to 1000 rpm, the higher temperature distribution starts at the region of higher melting point material *Al6061* and it is transmitted to the region of lower melting point material *Al2024* depending on the linear speed value. Hence, for rotating speed N=500 rpm, the higher temperature distribution is in the region of material *Al6061* for speed range from 2 to5 mm/s and then it is reflected to the region of material *Al2024* for speed range v > 5 mm/s.

On the other hand, the temperature distribution in the circle region of pin and shoulder in the weldment specimen for v = 25 mm/s and all range of rotating speed is presented in Fig. 17, taking into account that the aluminum alloy *Al6061* has a higher melting point T_m = 933K than the other *Al2024*, T_m = 775K.

For all rotating speed ranges from 250 to 2000 rpm, the higher range of temperature is observed at the region of contact surface between the lower surface of shoulder and specimen. Hence, a large heat is generated in this surface due to the higher friction resulted between the two surfaces. The pin region gave small temperature values as compared to the shoulder which has a large common area with weldment specimen than the pin.

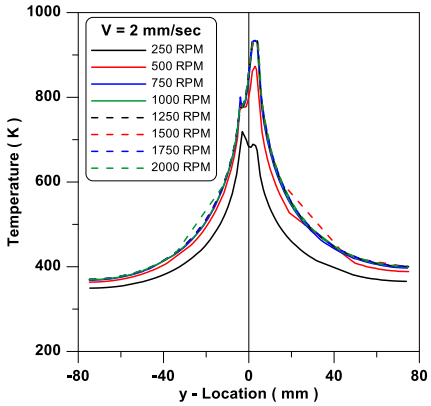

Fig. 9. Variation of temperature Y-axis, v = 2 mm/sec.

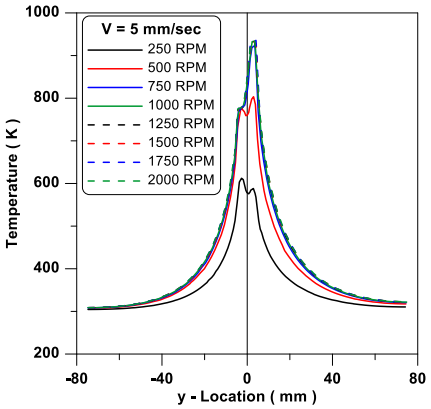

Fig.10. Variation of temperature, Y-axis, v = 5 mm/sec.

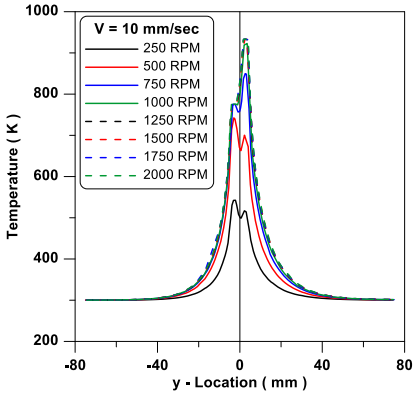

Fig. 11. Variation of temperature, Y-axis, v = 10 mm/sec.

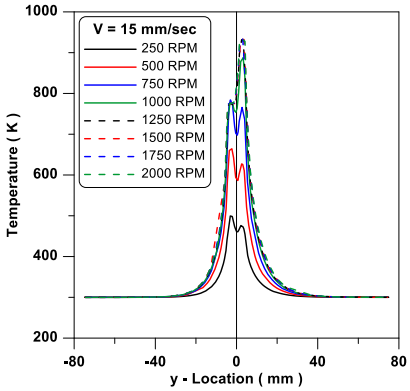

Fig. 12. Variation of temperature, Y-axis, v = 15 mm/sec.

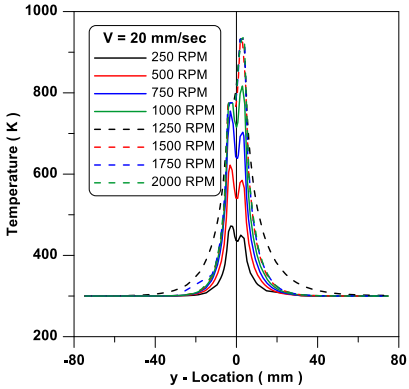

Fig. 13. Variation of temperature, Y-axis, v = 20 mm/sec.

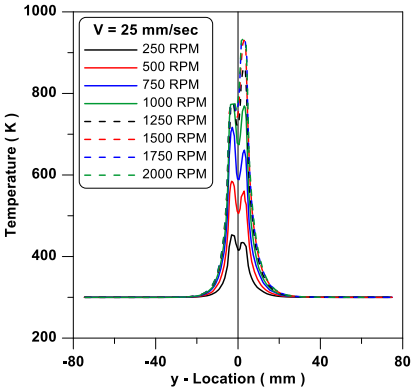

Fig. 14. Variation of temperature, Y-axis, v = 25 mm/sec.

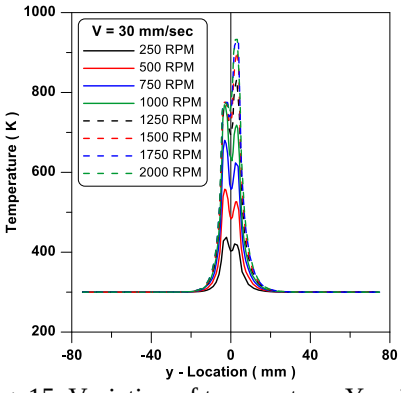

Fig. 15. Variation of temperature, Y-axis, v = 30 mm/sec.

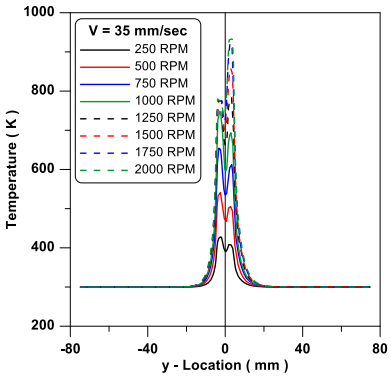

Fig. 16. Variation of temperature, Y-axis, v = 35 mm/sec.

For rotating speed values of 250, 500 and 750 rpm, the region of higher temperature range is observed in the common area between shoulder and the two materials (*Al6061, Al2024*). Approximately, this region is divided intoo two equal sectors for each material. Increasing the rotating speed resulted in increasing region of higher temperature range. Hence, the angle of sector increased with the rotating speed (114° for N=250 rpm, 134° for N=500 rpm and 154° for N=750 rpm). Exactly, the increasing in the sector angle is the same for each rotating speed step (angle= 20º for each N=250 rpm). For this range of rotating speed, the maximum temperature doesn't reach the melting point for both of materials (*Al6061, Al2024*).

For rotating speed values from 1000 to 2000 rpm, the region of higher temperature range transmitted to the common area between shoulder and the material (*Al6061*). The angle of sector increased with the rotating speed (70° for N=1000 rpm, 85° for N=1250 rpm, 130° for N=1500 rpm and 180° for N=1750, 2000 rpm). That means, when the sector angle reaches 180° at a specific higher rotating speed (N=1750 rpm), this angle will stop when the rotating speed increased.

4.2 Temperature distribution in the upper and lower surface

In order to know the difference of temperature between the upper and lower surface of weldment through the welding process, three samples have been considered. The first one with low speed condition (v =2 mm/s, N=250 rpm), the second with intermediate speed condition (v =15 mm/s, N=1000 rpm) and the third with high speed condition (v =35 mm/s, N=2000 rpm), Fig.18.

In general, the upper surface has large temperature values as comparing with the lower surface especially at the region of pin and shoulder circle. Hence, the upper surface has an additional heat generated due to the friction between it and the shoulder surface, while the lower surface has no shoulder friction. Away from this region, the temperature values are the same. This can be explained by the fact that the thickness of the plate is relatively small (t= 3 mm) which gives a uniform temperature distribution along it.

Increasing the speed values results in increasing the difference of temperature values between the upper and lower surface at the region of pin and shoulder circle. This is reason why the heat generated in pin and shoulder depends extremely on the speed, Eqs (2) and (3). Then, the higher rotating speed has a higher effect on this difference than the linear speed. The heat generated in the upper surface equals to those of shoulder and pin - Eqs. (2) and (3) - while the heat generated in the lower surface is from pin only. This heat is approximately the same for each material (*Al6061, Al2024*). Therefore, for the lower surface, a similar behavior of temperature distribution is found for each material.

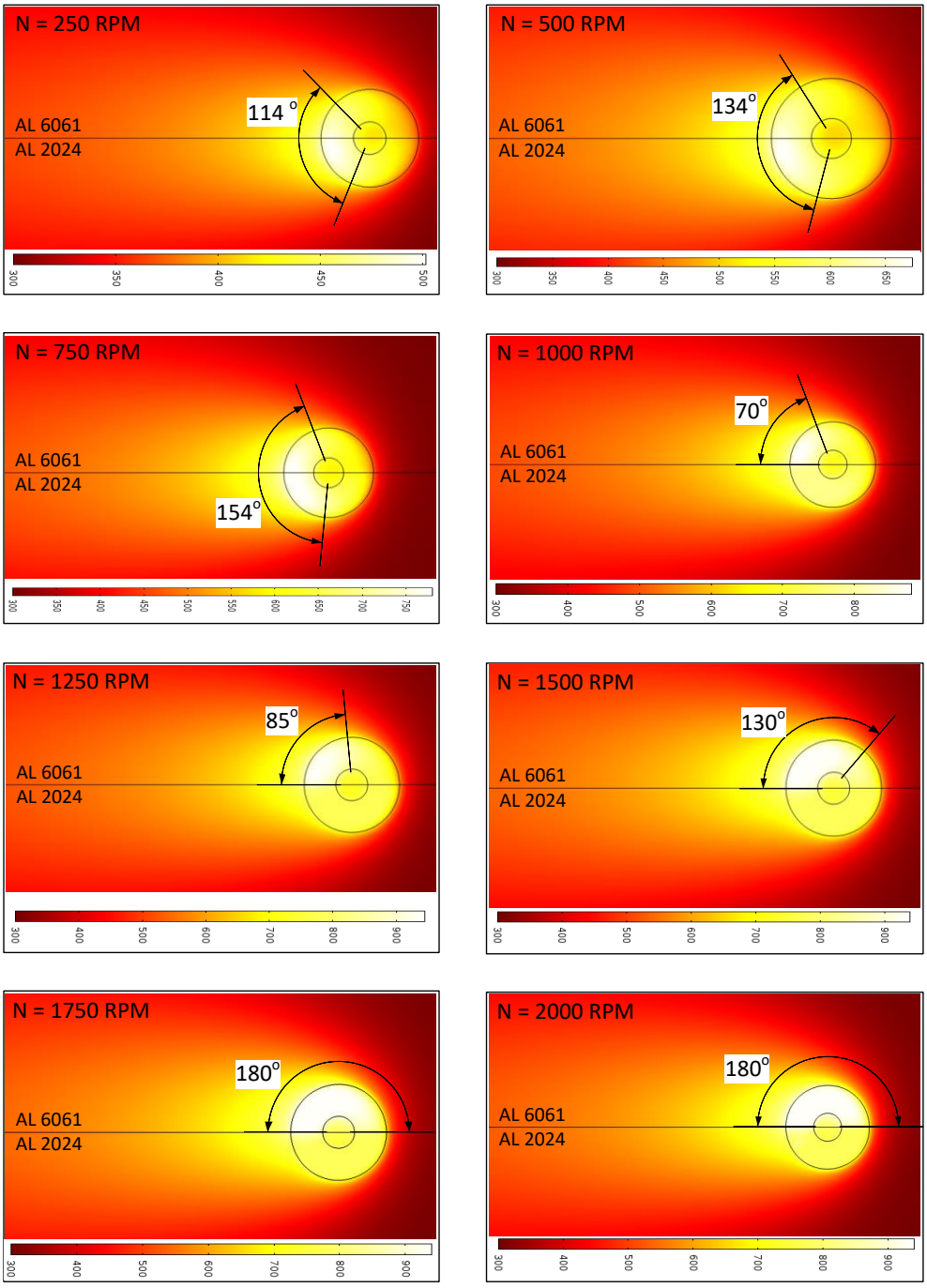

Fig. 17. Temperature distribution in the weldment specimen through region of pin and shoulder (v =25 mm/s)

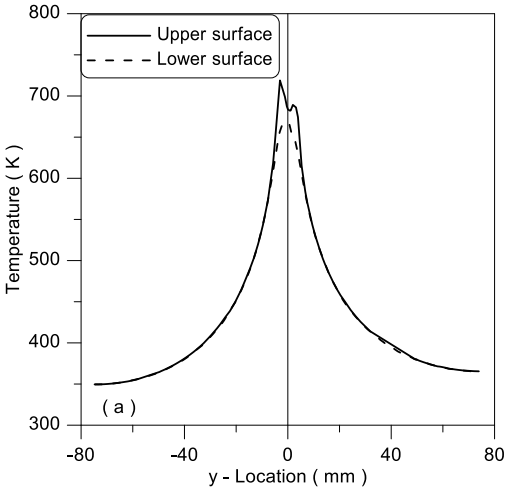

(a) v =2 mm/s, N=250 rpm

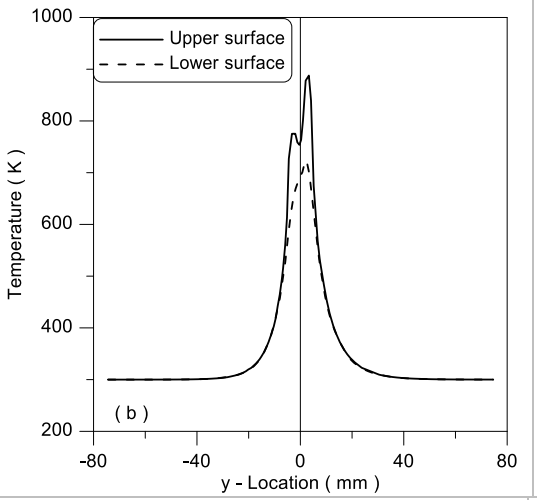

(b) v =15 mm/s, N=1000 rpm

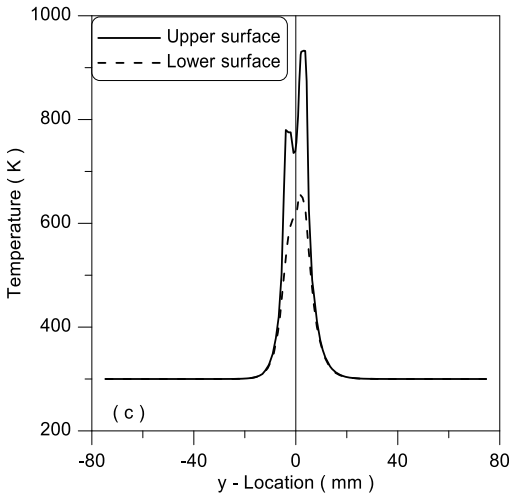

(c) v =35 mm/s, N=2000 rpm

Fig.18. Variation of temperature through the upper and lower surface

5. Conclusions

From the above results it can be concluded that the higher temperature field behaves like flame starting from the center of rotating tool and decreasing with linear speed.

The higher rate in temperature change is found through the weld line as comparing with the transverse line. Welding of different materials gave a non-symmetrical temperature distribution about the weld line. Increasing the linear speed gave a decrease in the temperature values. As well as increasing the rotating speed gave an increase in the temperature values, while increasing the higher rotating speeds has no effect on the temperature at low linear speed.

It can be observed that at low rotating speed, a higher temperature distribution is observed at the region of lower melting point material. At high rotating speed, a higher temperature distribution is observed at the region of higher melting point material. Finally, at intermediate rotating speed, the higher temperature distribution is the same for each material region.

The higher ranges of temperature lie at the region of contact surface between the shoulder and specimen. The pin region gave a small temperature values as compared with shoulder region. At the region of pin and shoulder, the upper surface has larger temperature values than those of lower surface. Increasing the speed values results in increasing this difference. At the lower surface an approximately symmetrical behavior of temperature distribution is found along the weld line. The FEM gave a good agreement with the experimental data.

[1].R E F E R E N C E S

[2]. *Sindo Kou,* (welding metallurgy), John Wiley & Sons. 2003.

[3]. *M. Grujicic, G. Arakere, H.V. Yalavarthy, T. He, C.-F. Yen, and B.A. Cheeseman,* Modeling of AA5083 Material-Microstructure Evolution during Butt Friction-Stir Welding, Journal of Materials Engineering and Performance, **Vol. 19,** no**.** 5, July 2010.

[4]. *D.Raguraman, D. Muruganandam, and L.A.Kumaraswamidhas,* Study of Tool Geometry on Friction Stir Welding OF AA 6061 and AZ61, Journal of Mechanical and Civil Engineering **Vol. 3**, 2014, pp. 63-69.

[5]. *S. Ji, Y. Jin, Y. Yue, L. Zhang1 and Z. Lv,* the Effect of Toll Geometry on Material Flow Behavior of Friction Stir Welding of Titanium Alloy, Engineering Review, **Vol. 33**, Issue 2, 2013, 107-113.

[6]. *Therese Källgren, thesis,* Friction Stir Welding of Copper Canisters for Nuclear Waste, Department of Materials Science and Engineering, M. Sc. Theses, Royal Institute of Technology, Sweden, 2005.

[7]. *G. Iacobescu* , A theoretical Model for Welding Process with Gaussian Heat Source – Part 1, U.P.B. Sci. Bull., Series D, **Vol. 68**, No. 4, 2006.

[8]. *ASTM* -Standard Specification for Aluminum and Aluminum-Alloy Sheet and Plate, ASTM B209, 1996.

[9]. *ASTM* –Standard, Test Methods of Tension Testing Wrought and Cast Aluminum- and Magnesium-Alloy Products, ASTM B557M-02a, 2003.

[10]. *ASTM*- ,Standard Specification for Tool Steels Alloy, ASTM A681 – 94, 1999.

[11]. *Jiji, Latif M., and Latif Menashi Jiji*. (Heat convection), New York: Springer, 2006.

[12]. *Lars-Erik Lindgren,* (Computational welding mechanics – Thermo mechanical simulations and microstructural), Woodhead Publishing Limited, 2007.

[13]. *P. Colegrove*, 3-Dimensional Flow and Thermal Modeling of the Friction Stir Welding Process, Proceedings of the 2nd International Symposium on Friction Stir Welding, Gothenburg, Sweden, 2000.
[14]. *Bejan, Adrian*. (Convection heat transfer), John wiley & sons, 2013.
[15]. *Jack P. Holman*, (Heat Transfer), McGraw-Hill Companies, Inc., 2010.